

# A Diffusion Process on Riemannian Manifold for Visual Tracking

Marcus Chen, Cham Tat Jen, Pang Sze Kim, Alvina Goh

**Abstract**—Robust visual tracking for long video sequences is a research area that has many important applications. The main challenges include how the target image can be modeled and how this model can be updated. In this paper, we model the target using a covariance descriptor, as this descriptor is robust to problems such as pixel-pixel misalignment, pose and illumination changes, that commonly occur in visual tracking. We model the changes in the template using a generative process. We introduce a new dynamical model for the template update using a random walk on the Riemannian manifold where the covariance descriptors lie in. This is done using log-transformed space of the manifold to free the constraints imposed inherently by positive semidefinite matrices. Modeling template variations and poses kinetics together in the state space enables us to jointly quantify the uncertainties relating to the kinematic states and the template in a principled way. Finally, the sequential inference of the posterior distribution of the kinematic states and the template is done using a particle filter. Our results shows that this principled approach can be robust to changes in illumination, poses and spatial affine transformation. In the experiments, our method outperformed the current state-of-the-art algorithm - the incremental Principal Component Analysis method [34], particularly when a target underwent fast poses changes and also maintained a comparable performance in stable target tracking cases.

**Index Terms**—Tracking, Particle filtering, Template update, Generative Template Model, Riemannian manifolds, log-transformed space.



## 1 INTRODUCTION

Visual tracking is an important vision research topic that has many applications, ranging from motion-based recognition [7], surveillance [18], human-computer interaction [10], etc. It also covers many aspects of computer vision problems, such as target feature representation [46], feature selection [9], and feature learning [15]. Even though it has been actively researched for decades, many challenges remain especially with changes in target poses and appearance, and illumination in a long video sequence. Figure 1 shows two simple examples of how a target can vary over a short time interval. Often these challenges are common and require a good solution in order for long stable tracking in many real life tasks. There are generally three common approaches to deal with target appearance variations. First is to use robust or invariant target features such as scale invariant feature transformation and color histogram [3]. However, as shown by Figure 1, target appearance can change significantly over time, and end up totally different from the starting frame due to variations in target poses and image illumination. The second approach is to employ a complete set of possible target models [4], aiming to model possible target variations.

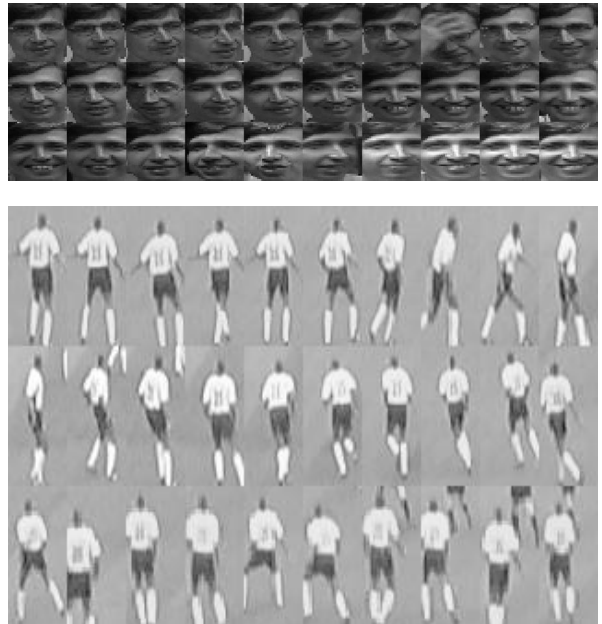


Fig. 1. Target patches for successive 871 frames, from #1, 31, ...871 from 2 video sequences. Target changes in both illumination, poses, appearances even after being affine warped to a standard size.

- Marcus Chen and Cham Tat Jen are with the Department of School of Computer Engineering, Nanyang Technological University, is with the Department.
- Pang Sze Kim and Alvina Goh are with DSO National Laboratories, Singapore.

However, this requires learning of the target model in advance and can hardly be scalable. Finally, the last approach is to update the template gradually as it evolves. Note that in this paper, we loosely use the term template for target representation, and do not strictly limit to the image patches. There are

several choices for a target template found in the literature. For example, [38] uses the histogram of oriented gradients, while [3] uses the color histogram, [45] L1 sparse representation, [23] active appearance model, [34] principal subspace of image patches, and [31] features covariance.

The template update problem can be expressed mathematically as Eqn. (1).

$$\overline{T}_t = f(T_t, \overline{T}_{t-1}) \quad (1)$$

where  $T_t, \overline{T}_t, t \in [1, 2, \dots]$  are the estimated and updated templates respectively at time  $t$ . However, as shown in [23], target template updating is a challenging task. According to [23], if the template was not updated at all, the template would become outdated shortly and cannot be used for matching as the target appearance would have undergone changes temporally. On the other hand, update at every frame would result in accumulation of small errors, and eventually a template drift and loss target information.

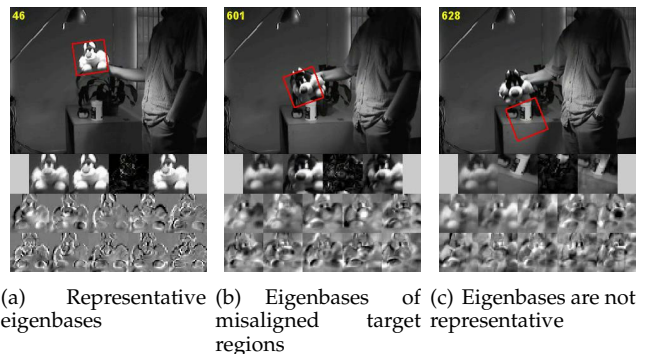
Recognizing the importance of template update, many methods have been proposed. One common and intuitive approach is to use linear updating function in the respective feature spaces, such as [31] on the covariance manifold. This will smoothen the changes between the estimated Template and updated template. Similarly, Kalman filter has also been used in [25] to track template features variables, but not target trajectory. On the other hand, there are three well-known template update algorithms in the literature, namely template alignment [23], Online Expectation and Maximization (EM) [19], and incremental subspace method [34]. Here, we briefly survey these three algorithms.

In template alignment method, [23] proposes a heuristic but robust criteria to decide whether to update the template at time  $t$ . The basic idea is to keep the starting template to correct the drift of the estimated template. The latest estimated template is first matched to the previous updated template. It is then warped before checking with the first template. For a small template displacement, this method works very well. However, by imposing alignment between the latest template and the first template, this method inherently limit target poses changes to a warping model.

The online EM method [19] employs a mixture of three template distributions to account for template variations, namely, *long term stable template*, *interframe variational template*, and *outlier template*. These templates model stable appearance of target, interframe changes in appearance of poses, and occlusion or outliers respectively. Employing a Gaussian mixture model, parameters and membership are estimated on the fly using online EM. In this framework, each pixel in the target patches is assumed to be independent and consequently more stable pixels tend to gain more weights in the similarity measure. This could

gradually drift the template in the presence of more stable background pixels.

The third algorithm is to represent the target in its eigenspace, proposed by [34]. The posterior estimates of the template are collected over an interval, and these estimates are then analyzed online through an Incremental Principal Component Analysis method(IPCA). This method can capture changes in template variation in eigenbases. The mean of the posterior estimates are also kept as stable templates. The authors have tested IPCA with various video sequences, and demonstrated its great robustness to the template variations due to pose changes and illumination changes. Figure 2 illustrates an incremental update of eigenbases and means. The images in the 3<sup>rd</sup> row show how the eigenbases evolve over time. It has been shown in the paper that the updated templates could almost reconstruct the original image samples over the sequence, reflecting the ability of the eigenbases to model temporal variations. Although IPCA is often very robust and can track target very accurately even in noisy, low contrast image sequences, IPCA falls short when the target undergoes fast pose changes and dramatic illumination changes as stated on the paper. This may be because PCA inherently assumes that the target templates over time are from a Gaussian distribution. In abrupt changes in poses and illumination, this assumption does not hold. The unimodal distribution also requires good pixel-wise alignment between the posterior estimate and eigenbases, otherwise uncertainties in template alignment would contribute to template variance and may lead to non-informative basis. A good example from the paper is shown in Figure 2. One can see that from frames #600 to #636, the eigenbases are not representative anymore and the tracker loses track of the target.



(a) Representative eigenbases (b) Eigenbases of target are not representative (c) Eigenbases are not representative

Fig. 2. Results of incremental subspace method on the Sylvester sequence. Pixel-wise misalignment could render eigenbasis non-representative. The 1<sup>st</sup> row are the sample frames. The 2<sup>nd</sup> row images are the current sample mean, tracked region, reconstructed image, and the reconstruction error respectively. The 3<sup>rd</sup> and 4<sup>th</sup> rows are the top 10 principal eigenbases.

So far, most of the current state-of-the-art algorithms update templates in an out-of-chain manner, by assuming the posterior estimate is “good enough” for template update with pixel-wise alignment. If the target poses posterior estimate is inaccurate or there is a mis-alignment between the estimated and last updated template, the update methods will gradually drift. On the other hand, if the template update is not good, then the posterior estimate of target poses is unlikely to be accurate. These coupled dual problems often render these methods unable to track well when the targets undergo fast changes in poses or non-rigid transformation. However, robustness to fast target poses has many real life applications such as human tracking, maritime target tracking, etc.

To solve these dual problems faced by the existing state-of-the-art algorithms, [8] introduces a novel approach to simultaneously quantify these two uncertainties by including both of them into the state space of a Bayesian framework, instead of just target poses in the exist methods. In this manner, no posterior estimate is used for updating, instead better matched multiple hypothesized templates are propagated automatically.

**Paper contributions.** To the best of our knowledge, almost all the state-of-art algorithms use out-of-chain template updating methods. That is to say, the updating of template model is done after obtaining the posterior estimate of the targets position. In this paper, we propose a method to update target model in tandem with the target kinematics. In other words, we model the target template as a part of the state space. We choose the covariance descriptor for the target descriptor as it is more robust to problems such as pixel-pixel misalignment and changes in pose and illumination. Since positive definite covariance matrices form a Riemannian manifold, we model the target template model variation by a random walk on the covariance Riemannian manifold. We propose a novel superior template propagation mechanism in the log-transformed space of the manifold to free the constraints imposed inherently by positive semidefinite matrices, leading to a greater ability in dealing with template variations. Our resultant method outperforms the state-of-the-art Incremental PCA algorithm [34] in dealing with fast moving and changing targets, as will be clearly shown in the experiments section.

The paper is organized as follows: Section 2 gives a brief introduction to both covariance descriptors and Riemannian manifold, Section 3 gives a Bayesian formulation of simultaneous inference of both target kinetics and template posterior distribution, Section 4 analyzes the template generative process. In Section 5, we empirically compare our results with IPCA and give a short discussion. Finally, section 6 concludes this paper.

## 2 TARGET COVARIANCE DESCRIPTOR

In this section, we explain the motivation of using covariance descriptor and its operation on Riemannian manifold.

### 2.1 Covariance Descriptor

A covariance descriptor is defined as follows:

$$C = \frac{1}{N-1} \sum_{i=1}^N (f(i) - \bar{f}) (f(i) - \bar{f})^T \quad (2)$$

where  $f$  is a feature vector,  $\bar{f} = \frac{1}{N} \sum_{i=1}^N (f(i))$  is the mean of the feature vector over  $N$  pixels in the target region. In this paper, we use the following 9-dimensional feature vector:

$$f(i) = \left[ x_w, y_w, I(x_w, y_w), |I_{x_w}|, |I_{y_w}|, \sqrt{I_{x_w}^2 + I_{y_w}^2}, \arctan \frac{|I_{x_w}|}{|I_{y_w}|}, |I_{x_w x_w}|, |I_{y_w y_w}| \right]. \quad (3)$$

They are  $x, y$  coordinates, pixel intensity,  $x, y$  directional intensity gradients, gradient magnitude and angle, and second order gradients respectively.  $w$  denotes that these features are extracted after warping image patches to a standard size.

Since its proposed use in human detection [40], covariance descriptor has gained popularity for many applications, such as face recognition [26], license plate detection [30], and tracking [31], [45]. Some main advantages of choosing the covariance descriptor [42] to model the template include its lower dimensionality of  $\frac{1}{2}(d^2 + d)$  (45 in this paper as  $d = 9$ ), compared to its number of target pixels ( $32 \times 32 = 1024$  in this paper), its ability to fuse multiple possibly correlated features, and its robustness to match targets in different views and poses.

By its definition, covariance matrix is clearly a positive semi-definite matrix, which lies on a Riemannian manifold. We will now briefly explain some basic operations on the Riemannian manifold.

### 2.2 Riemannian Manifold

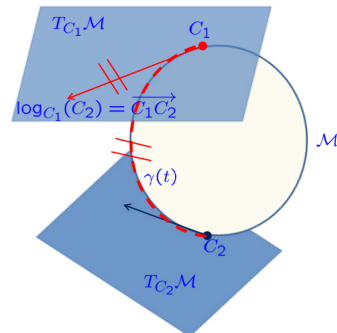


Fig. 3. The geodesic distance is the norm of a vector on the tangent space  $T_{C_1}\mathcal{M}$  of at point  $C_1$  on the manifold  $\mathcal{M}$

TABLE 1  
Operations in Euclidean and Riemannian spaces

Euclidean space	Riemannian manifold
$C_j = C_i + C_i \vec{C}_j$	$C_j = \exp_{C_i}(C_i \vec{C}_j)$
$\vec{C}_i \vec{C}_j = C_j - C_i$	$\vec{C}_i \vec{C}_j = \log_{C_i}(C_j)$
$\text{dist}(C_i, C - j) = \ C_j - C_i\ $	$\text{dist}(C_i, C_j) = \ C_i \vec{C}_j\ _{C_i}$

219 A Riemannian manifold  $\mathcal{M}$  is a differential mani-  
220 fold and each of its tangent space  $T_{C_i}\mathcal{M}$  has a metric  
221 function  $g$  which defines the dot products between  
222 any two tangent vectors  $y_k, y_l$ . The covariance descrip-  
223 tor is a point on the manifold  $\mathcal{M}$ , the following opera-  
224 tions can be applied to it. The Riemannian metric:

$$225 \langle y_k, y_l \rangle_{C_i} = \text{trace} \left( C_i^{\frac{1}{2}} y_k C_i^{-1} y_l C_i^{-\frac{1}{2}} \right). \quad (4)$$

227 The exponential map  $\exp_{C_i} : T_{C_i}\mathcal{M} \rightarrow \mathcal{M}$ , takes a  
228 tangent vector at point  $C_i$  and maps to another point  
229  $C_j$ :

$$230 C_j = \exp_{C_i}(y) = C_i^{1/2} \exp \left( C_i^{-\frac{1}{2}} y C_i^{-\frac{1}{2}} \right) C_i^{\frac{1}{2}}, \quad (5)$$

232 The inverse of the exponential map is the logarithm  
233 map, which takes a starting point  $C_i$  and destination  
234  $C_j$ , maps to the tangent vector  $y$  at point  $C_i$ .

$$235 y = \log_{C_i} C_j = C_i^{\frac{1}{2}} \log \left( C_i^{-\frac{1}{2}} C_j C_i^{-\frac{1}{2}} \right) C_i^{\frac{1}{2}}. \quad (6)$$

237 Finally, the distance between two covariance matrices  
238  $C_i$  and  $C_j$  is given as:

$$239 d(C_i, C_j) = \sqrt{\sum_{k=1}^d \ln^2 \lambda_k(C_i, C_j)}, \quad (7)$$

241 where  $\lambda_k(C_i, C_j)$  are the generalized eigenvalues of  
242  $C_i$  and  $C_j$ . That is,  $\lambda_k C_i v_k - C_j v_k = 0$ , and  $d$  is the  
243 dimension of the covariance matrices.

244 Note that  $\exp_{C_i}(\cdot)$  and  $\log_{C_i}(\cdot)$  are maps on the  
245 Riemannian manifold, whereas  $\exp(\cdot)$  and  $\log(\cdot)$  de-  
246 note the normal matrix exponential and logarithmic  
247 operations. Both  $\exp_{C_i}(y)$  and tangent vector  $y$  are  
248 both  $d \times d$  matrices in this paper.

### 249 2.3 Motivation of Manifold Modeling

250 High dimensional image data often lies in low dimen-  
251 sional manifold. For an example, a collection of  
252 rotated handwriting zeros in Figure 4 lie in a dimen-  
253 sion of  $28 \times 28 = 784$  using vectorized representation,  
254 but have only one rotational parameter. Popular dimen-  
255 sional reduction methods such as ISOMAP [39],  
256 eigenmap [2], LLE [35] model data using manifold  
257 structures. In visual tracking, the target patches in  
258 the image sequence are implicitly bounded by the  
259 target's degree of freedom captured by images, such  
260 as rotation, translation, scaling etc. These implicit  
261 parameters modeled using low dimensional manifold  
could capture image distance. The simplest and yet

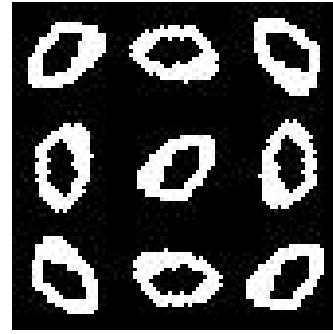
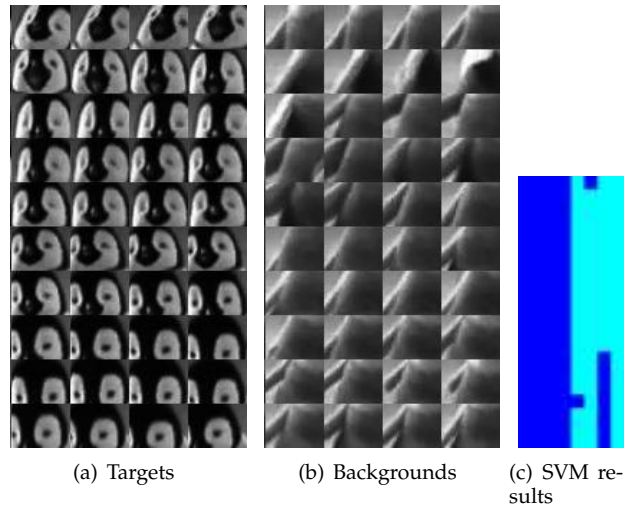


Fig. 4. A collection of rotated handwriting zeros by the angle of  $45^\circ$  each time.



(a) Targets (b) Backgrounds (c) SVM results  
(d) Euclidean distance (e) Manifold distance

Fig. 5. An illustration of distance between images can be better modeled on a manifold, a sequence of dancing penguin from youtube. In (d), Euclidean distance between targets is larger than the distance between target and background; and not on the manifold space. Furthermore, in (e), SVM cannot linearly separate the targets from backgrounds in vectorized Euclidean space.

most popular distance measure between images is Euclidean distance between the vectorized images. A simple example of the head of dancing penguin from youtube is adopted to illustrate in Figure 5 that the manifold of covariance descriptor can model the image distance better and can separate target patches from the background better. Using Euclidean distance, the distance between target patches and first target

patch could be larger than the one between the background and the first target patch. Furthermore, a test of support vector machine using linear kernel showed that some background patches are classified into the target patches. On the other hand, the separation between target patches and background patches were separated shown in Figure 5e.

### 3 BAYESIAN FRAMEWORK

In this section, we use a standard Bayesian framework [33] to formulate tracking of both template and kinetics as follows:

$$P(C_t, \mathbf{s}_t | z_{1:t}) \propto P(z_t | C_t, \mathbf{s}_t) \int P(\mathbf{s}_t, C_t | \mathbf{s}_{t-1}, C_{t-1}) P(C_{t-1}, \mathbf{s}_{t-1} | z_{1:t-1}) d\mathbf{s}_{t-1} dC_{t-1}, \quad (8)$$

where  $z_t$  is the measurement,  $\mathbf{s}_t$  is the kinetic state variables,  $C_t$  is the covariance descriptor,  $P(C_t, \mathbf{s}_t | z_{1:t})$  is the posterior probability of target template and pose given the measurement,  $P(z_t | C_t, \mathbf{s}_t)$  is the observational model, and  $P(\mathbf{s}_t, C_t | \mathbf{s}_{t-1}, C_{t-1})$  is the dynamical model. They are further elaborated in the following subsections.

#### 3.1 Dynamical Model

The state space in our paper includes both target kinetic variables  $\mathbf{s}_t$  and template covariance descriptor  $C_t$ . The state variables are defined in Eqns. (9) and (10), and we would like to estimate them through the Bayesian framework in Eqn.(8). These state variables are propagated from time  $t-1$  to  $t$  through a dynamical model  $P(\mathbf{s}_t, C_t | \mathbf{s}_{t-1}, C_{t-1})$ .

$$\mathbf{s}_t = [x_t, y_t, \dot{x}_t, \dot{y}_t, h_t, \theta_t], \quad (9)$$

$$C_t = \text{cov}(x_w, y_w, I(x_w, y_w), |I_{x_w}|, |I_{y_w}|, \arctan \frac{|I_{y_w}|}{|I_{x_w}|}, \sqrt{I_{x_w}^2 + I_{y_w}^2}, |I_{xx_w}|, |I_{yy_w}|), \quad (10)$$

where  $x_t, y_t$  are the spatial coordinates of the target center position at time  $t$ ,  $\dot{x}_t, \dot{y}_t$  are the velocities,  $h_t$  is the scaling factor, and  $\theta_t$  is the orientation.  $x_w, y_w$  are the coordinates of a pixel on the standard target patch warped from  $x_t, y_t$ ,  $I(x_w, y_w)$  is the pixel intensity and  $\{I_{x_w}, I_{y_w}\}$  are the patch intensity gradients,  $\{I_{xx_w}, I_{yy_w}\}$  are the second order gradients. Assuming independence between kinetic variables and covariance, we model the joint dynamics as follows:

$$P(\mathbf{s}_t, C_t | \mathbf{s}_{t-1}, C_{t-1}) = P(\mathbf{s}_t | \mathbf{s}_{t-1}) P(C_t | C_{t-1}), \quad (11)$$

$$\mathbf{s}_t = k(\mathbf{s}_{t-1}) + u_t, \quad (12)$$

$$C_t = \exp_{C_{t-1}}(n_t). \quad (13)$$

$k$  is the kinetic model and we use a near constant velocity linear model  $k(\mathbf{s}_{t-1}) = A\mathbf{s}_{t-1}$ .  $u_t$  is generated with an interacting Gaussian models with a jumping probability of  $[0.9, 0.1]$  to model sudden changes in target poses. As for template dynamical model,

$n_t \in T_{C_t} \mathcal{M}$  is a random process on the tangent plane of manifold  $\mathcal{M}$ . An example of this could be the Brownian motion process as described by [17]. In this paper, we choose to model the template dynamical model in log-transformed space of the manifold as follows:

$$C_t = \exp(\log(C_{t-1}) + w_t) \quad (14)$$

$$\text{where } w_t \sim N(0, \Sigma), \Sigma_{i,j} = \Sigma_{j,i} \sim N(0, \sigma_{i,j}^2) \quad (15)$$

$$P(\log(C_t)) \propto \exp\left(-\frac{1}{2} \sum_{i \leq j, i, j \in [1, d]} \frac{w_t(i, j)^2}{\sigma_{i,j}^2}\right) \quad (15)$$

where  $w_t$  is simply a random symmetric matrices and  $N(0, \sigma_{i,j}^2), i, j \in [1, d]$  are normal distributions. According to [1], the matrix exponential function maps a symmetric matrix to its corresponding positive semi-definite,  $\exp: \text{Sym}(d) \rightarrow \text{Sym}^+(d)$ , and it is one-to-one mapping. As such, the generated samples of  $C_t$  is always a positive semi-definite (PSD) matrix. This frees the inherent constraints of positive eigenvalues in a PSD matrix. This distribution may be considered as a log-normal distribution of the PSD matrices as defined in [36].

$$\begin{aligned} & C_t^{-1} C_{t-1} \\ &= \exp(-\log(C_{t-1}) - w_t) \exp(\log(C_{t-1})) \\ &= \exp(-w_t) \end{aligned} \quad (16)$$

Generalized Eigenvalues:

$$\begin{aligned} \lambda_k C_t v - C_{t-1} v &= 0 \\ C_t^{-1} C_{t-1} v &= \lambda_k v \\ \exp(-w_t) v &= \lambda_k v \\ d(C_{t-1}, C_t) &= \left[ \sum_{k=1}^d [\ln^2 \lambda_k (\exp(-w_t))] \right]^{1/2} \\ &= \left[ \sum_{k=1}^d \lambda_k^2(w_t) \right]^{1/2}, \text{ if } \exists w_t^{-1} \end{aligned} \quad (17)$$

In this paper, for  $d = 9$ ,  $w_t$ 's eigenvalues  $\lambda_1(w_t) \geq \lambda_2(w_t) \geq \dots \geq \lambda_9(w_t)$  can be bounded according to [47], assuming the entries of the noise matrix are bounded by  $[a, b]$ , i.e.  $a \leq w_t(i, j) \leq b$ :

$$\lambda_9(w_t) \geq \begin{cases} \frac{1}{2} (9a - \sqrt{a^2 + 80b^2}) & |a| < b \\ 9a & \text{otherwise.} \end{cases} \quad (18)$$

$$\lambda_1(w_t) \leq \begin{cases} \frac{1}{2} (9b + \sqrt{a^2 + 80b^2}) & |a| < b \\ 9b & \text{otherwise.} \end{cases} \quad (19)$$

In other words, the eigenvalues are roughly within an order of magnitude of  $\max(\sigma_{i,j})$  for this random process. In this way, the template diffusion spread on the manifold can be easily managed by choosing an appropriate  $\max(\sigma_{i,j})$  in  $w_t$ .

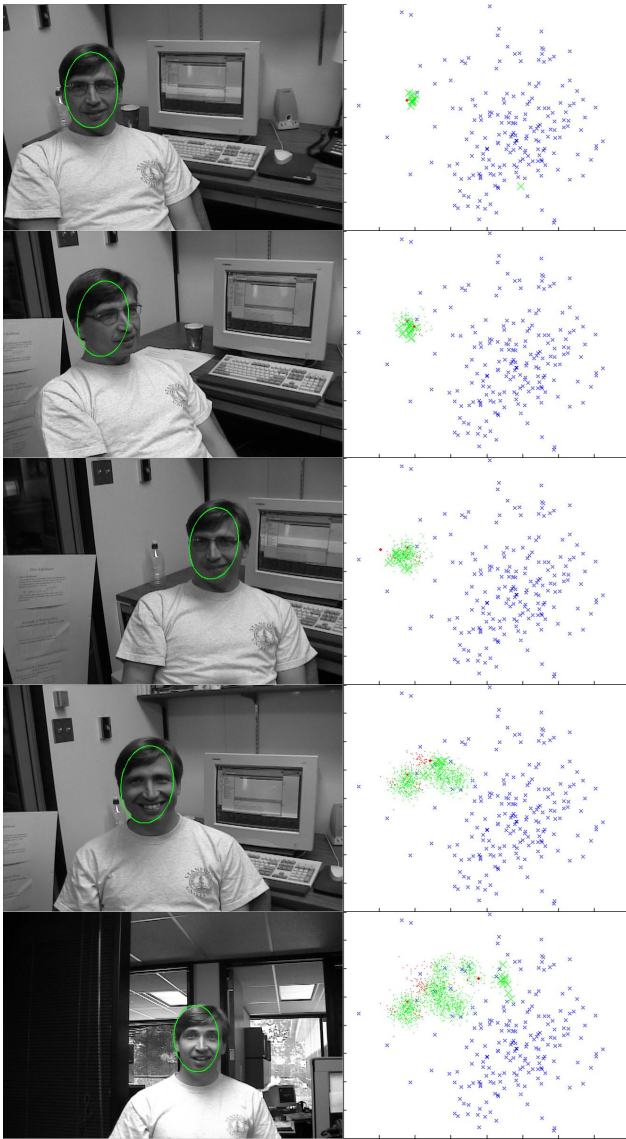


Fig. 6. Evolution of template and generated templates, frame #1, 101, 201, 501, 801, Green cross: top 10 similar generated templates, Red: ground truth, Blue cross: the background.

411

### 3.2 Observation Model

The observation model  $P(z_t|C_t, s_t)$  measures the likelihood of a target given target poses and template values, it is modeled as follows:

$$P(z_t|C_t, s_t) \sim N(0, \sigma^2), \quad (20)$$

$$z_t = d(C_t, C_t^*),$$

$$C_t^* = g(s_t, \text{Image}),$$

$$P(z_t|C_t, s_t) \propto \exp\left(-\frac{1}{2\sigma^2}d^2\right) \quad (21)$$

Here,  $d(C_t, C_t^*)$  is given by Eqn. (7).  $g$  is the covariance computation operator;  $g$  takes the kinetic value  $s_t$  of each particle at time  $t$ , warps the region to a standard size (in this paper,  $32 \times 32$ ) before computing covariance.

### 3.3 Overall Framework

We use a standard particle filter to do sequential inference. The particle filter [5], [33], [16] represents the distribution of state variables by a collection of samples and their weights. The advantage of using a particle filter is that it can deal with non-linear system and multi-modal posterior. The algorithm of the particle filter is as follows:

- 1) **Initialization.** The particle filter is initialized with a known realization of target state variables. This includes the target initial state values. Covariance of the target  $C_0$ , i.e. initial template is extracted for comparison later. The parameters of covariance generative process, i.e. template dynamical model are also determined.
- 2) **Propagation.** Each particle is propagated according to the propagation model in Eqns. (12) and (14). Both kinetic variables and template are generated through these random processes.
- 3) **Measure the likelihood.** At each particle  $i$ , the covariance descriptor  $C_t^*(i)$  extracted is compared to its corresponding template  $C_t(i)$ . The likelihood of the particle is then estimated as given in Eqn. (21).
- 4) **Posterior estimation.** The posterior estimate gives the estimate of the current target state, given all its previous information and measurements. This could be maximum a posteriori probability estimate or minimum mean square error estimate (MMSE). In this paper, we use MMSE.
- 5) **Resampling.** To avoid any degeneracies, resampling is conducted to redistribute the weight of particles.
- 6) **Loop.** Repeat the process from step 2 to 5 as time progresses.

### 4 ANALYSIS OF TEMPLATE GENERATIVE PROCESS

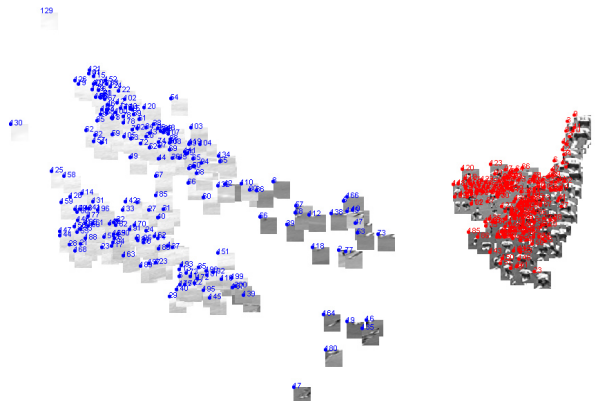


Fig. 7. Visualization of target in "soccer" sequences on the covariance manifold, Red: target patches, Blue: background patches.

In this section, we show that the covariance descriptor is a good representation of the target as well as the motivation behind performing a random walk as given in Section 3.1. Two reasonable criteria for a good target representation are as follows:

- the representation evolves gradually as the target undergoes changes in poses, appearance etc,
- there is clear separation of target and background.

To help visualize the distribution of target covariance matrices on the manifold, we use multidimensional scaling [21] to construct a visualization of the distribution of the covariance matrices. The distance matrix is constructed using Riemannian distance as given in Eqn.(7). The visualization shows the relative positions of targets (red) and backgrounds(blue). Visualizing the PETS 2003 Soccer sequence and Dudek Face sequence in Figures 7 and 6, we noticed that our representation of the targets tended to cluster together as they evolved gradually. This evolution is smoother and easier to model on the manifold as compared to the evolution of its original feature values at each pixel. This observation motivated us to model the template variations by using a random walk on the Riemannian manifold. Based on Eqns.(12) and (14), Figure 6 illustrates a realization of the random walk. This shows that our template dynamical model can model the actual target appearance variations. Changes in facial expression and face poses cause covariance template (shown as red points) to evolve slowly on the manifold, and they are well modeled by the generated covariances on the manifold (shown as green points).

## 5 EXPERIMENTS AND RESULTS

### 5.1 Experimental data

We tested our algorithm on some of popular tracking datasets, David Ross’s sequences including plush toy (toy Sylv), toy dog, david, car 4sequences from his website, Dudek Face sequences, and vehicle tracking sequences from PETS2001, soccer sequence from PETS2003. The test data information is tabulated in Table 2.

### 5.2 Performance measure

As spelled out in [22], a good measure should include both overall tracking and goodness of track. This paper uses the ratio between on-track length and sequence length to capture the performance of overall tracking, and on-track accuracy for goodness of track. Define tracking errors as:  $e_x(t) = \|g_x(t) - x(t)\|$ ,  $e_y(t) = \|g_y(t) - y(t)\|$ , where  $e_x(t), e_y(t), g_x(t), g_y(t)$  are the errors in  $x, y$  and ground truth in  $x, y$  at time  $t$

respectively.

$$\gamma_{ontrack} = \frac{1}{2} \left( \frac{e_x(t)}{H_x(t)} + \frac{e_y(t)}{H_y(t)} \right) \leq 1 \quad (22)$$

$$r_{ontrack} = \frac{\gamma_{ontrack}}{l} \quad (23)$$

$$rms_{ontrack} = \sqrt{\left( \frac{e_x(t)}{H_x(t)} \right)^{1/2} + \left( \frac{e_y(t)}{H_y(t)} \right)^{1/2}} \quad (24)$$

$H_x(t), H_y(t)$  are the ground truth target size at time  $t$ . In this work, ground truth on the target center is manually annotated, the target size is assumed to as those of the first frame (this may not be applicable to frames with a large change in target size).

### 5.3 Results and discussion

We compared our method with the current state-of-the-art algorithm, the incremental PCA (IPCA) method by David et al [34]. Our results are shown in red and the IPCA in green from Figures 9 to 15. In PLUSH TOY SYLV sequences shown in Figure 9, the IPCA failed to recover tracking from frame #609 when it locked onto the background, which looks more similar to the upright SYLV. Fast poses changes around frame #609 caused the IPCA eigenbases non-representative as shown in Figure 4.

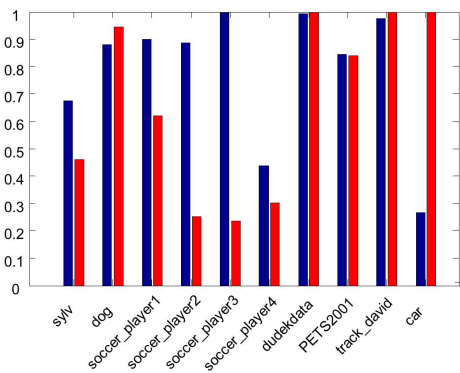
Similarly, in Figure 10, the IPCA failed to follow through when target underwent a fast motion towards the frame #1351. This shortcoming of the IPCA is better reflected in Soccer Sequences of PETS2003. the IPCA started to drift off from frame #628 shown in Figure 11 when the player moved his legs fast, and lost track shortly. In the same sequence in Figure 12, the IPCA found it hard to track the opposite team players who wore dark clothes after a short occlusion at frame #285.

In Figure 13, Dudek Face sequences, both methods perform well despite of his rich facial expressions, which have more effects on our covariance descriptor. In the more stable vehicle sequence from PETS2001 in Figure 14, again both methods could track well. Figure 15 shows an example of a car sequence, in which our method did not perform satisfactorily. Our method locked onto the background whereas the IPCA showed robustness to the illumination changes. The possible explanation is that our template dynamics was unable to account for this dramatic and non-smooth transition of the template when the car went into a shadowed region. Also, a closer look showed that the IPCA eigenbasis looked similar to the target template in shadows.

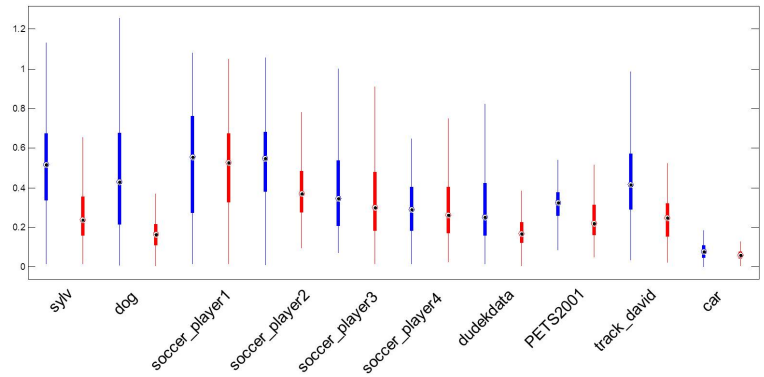
The overall tracking performance on the test cases is summarized in Figure 8. Note that images sequences of Sylv, PETS2001 and soccer player 4 have targets out of the images, this explained the small track duration performance. Nevertheless, our method shown in red generally had longer track length. On the hand, given frames that were on

TABLE 2  
Test Sequences

Test sequences	Source	No. of frames	Characteristics
Plush Toy (Toy Sylv)	David Ross	1344	fast changing, 3D Rotation, Scaling, Clutter, large movement
Toy dog	David Ross	1390	fast changing, 3D Rotation, Scaling, Clutter, large movement
Soccer player 1	PETS 2003	1000	Fast changing, white team, good contrast with background, occlusion
Soccer player 2			
Soccer player 3			
Soccer player 4			
Dudek Face Sequence	A.D. Jepson	1145	Fast changing, gray(red) team, poor contrast with background, occlusion
Truck	PETS 2001	200	Relatively stable, occlusion, 3D rotation
David	David Ross	503	relatively stable, scaling
Car 4	David Ross	640	relatively stable 2D rotation
			Relatively stable, scaling, shadow, specular effects



(a) Track duration rate  $r_{ontrack}$



(b) Track accuracy  $rms_{ontrack}$

Fig. 8. The results statistics, our results in blue, IPCA in red.

516 track for both trackers, IPCA showed better track  
 517 accuracy shown in Figure 8b. For the sequences with  
 518 frequent changes in target appearance such as soc-  
 519 cer sequences, the track goodness was comparable.  
 520 The video sequences may be found on the website,  
 521 <http://www.youtube.com/watch?v=KaSrVbGyvq4>.

522 **Discussion.** In stable tracking cases, good pixel-wise  
 523 alignment enabled the IPCA to track very well. The  
 524 IPCA was generally very robust to blurring, even illu-  
 525 mination changes, as eigenbasis tended to encompass  
 526 these changes. In other words, some eigenbasis looked  
 527 similar to blurred or illumination-changed templates.  
 528 The distance measure in the IPCA uses a norm of all  
 529 corresponding pixels difference; as such, it tends to be  
 530 very stable and well aligned in the stable target cases.  
 531 On the other hand, it is likely to favor the relatively  
 532 stable regions in the target. When such regions are too  
 533 similar to the background and target poses changes  
 534 at the same time, then the IPCA may lose track very  
 535 quickly in the Soccer Sequence in Figure 12. On the  
 536 other hand, our method uses covariance of gradients  
 537 and intensity; the template feature descriptor is much  
 538 smaller in dimension. This may cause our method  
 539 slightly less precise than the IPCA shown in Figure  
 540 10, which our method did not match to pixel accuracy.  
 541 Figure 15, our method lost track when the vehicle  
 entered the shadowed region, because the both gra-

543 dients and intensity changed significantly and for an  
 544 interval.

545 Although our method was slightly not as precise  
 546 in the stable cases, it gain much more flexibility in  
 547 the non-stable tracking scenarios. In the cases of non-  
 548 rigid or fast motion of targets, mis-alignment in the  
 549 posterior estimate (the new template sample to add  
 550 to the eigen space in the IPCA) and eigenbases may  
 551 accumulate over a short interval and consequently  
 552 render eigenbases non-representative at all. This in-  
 553 evitably leads to loss in tracking. Our method could  
 554 deal with these scenarios a lot better for two rea-  
 555 sons. Firstly, the template descriptor did not require  
 556 pixel-wise alignment and is robust to mis-alignment.  
 557 Secondly, the generative process could accommodate  
 558 multiple hypothesis of the template on the covariance  
 559 Riemannian manifold, and it automatically selects the  
 560 better hypothesis as the target template evolves as  
 561 shown in Figure 6.

562 However, there are some limitations in our algo-  
 563 rithm. One of them is to the need to carefully choose a  
 564 suitable region for tracking. Since we used the pub-  
 565 lished features such as intensity and gradients, and  
 566 second order gradients for covariance, these features  
 567 are sensitive to specular effects, dark shadows as  
 568 shown in Figure 15. It is also important to choose  
 a target region with fairly good gradients varia-

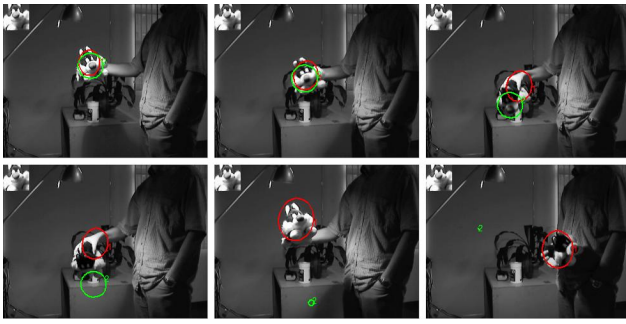


Fig. 9. Tracking results on PLUSH TOY SYLV sequences, frame #133, 594, 609, 613, 957, 1338, Green: IPCA, Red: our results. The IPCA failed to recover track from frame # 609.

570 tions, otherwise the covariance descriptor may be ill-  
 571 conditioned consequently affecting both eigenvalues  
 572 estimation and distance measurements in Equation  
 573 (7).

## 574 6 CONCLUSION

575 In this paper, we have proposed a new method to  
 576 update target model in tandem with the target kinem-  
 577 atics. More precisely, we have developed a gener-  
 578 ative template model in a principled way within a  
 579 Bayesian framework. A novel template propagation  
 580 mechanism in the log-transformed space of the co-  
 581 variance manifold to free the constraints inherently  
 582 imposed by positive definite matrices. We have shown  
 583 that the simple generative process can allow template  
 584 to evolve naturally with target appearance variation.  
 585 It is hoped that by jointly quantifying the uncertainties  
 586 of the target kinematics and template, we are able to  
 587 achieve more robust visual tracking. We have chosen  
 588 the covariance descriptor as the target representation.  
 589 We have modeled the target template model dynamic  
 590 using a random walk on the covariance Riemannian  
 591 manifold. Our template dynamic model is an example  
 592 of a diffusion process on the covariance Riemannian  
 593 manifold. In the experiments, our algorithm outper-  
 594 formed with the current state-of-the-art algorithm  
 595 IPCA particularly when the target underwent a fast  
 596 and non-rigid poses changes, and also maintained a  
 597 comparable performance when the target was more  
 598 stable. Some future work includes automatic selection  
 599 of covariance features that are more robust to a sud-  
 600 den dramatic change in illuminations.

601 Future work includes addressing a number of ques-  
 602 tions such as how should the diffusion speed be  
 603 adjusted and can the diffusion process be better con-  
 604 strained. Another area of work is to deal with illu-  
 605 mination changes in the manifold generative process.  
 606 In order to improve the goodness of track, a more  
 607 discriminative target descriptor is to be explored.

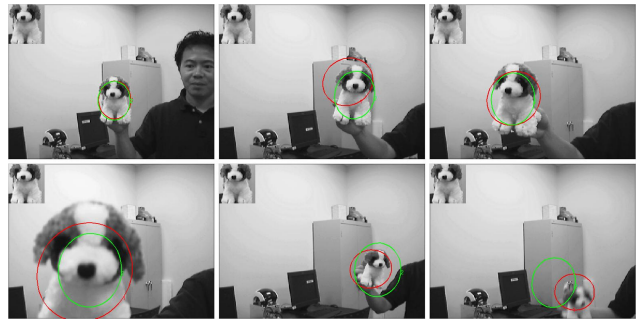


Fig. 10. Tracking results on toy dog sequences, frame #1, 450, 715, 1014, 1271, 1351, Green: IPCA, Red: our results. The IPCA was slightly more localized in stable case, but failed to follow through when the target underwent a fast motion towards frame #1351.

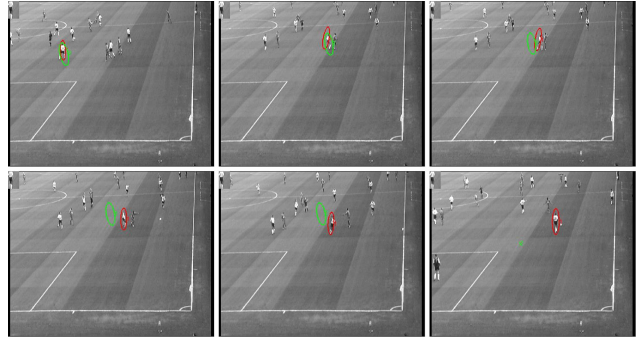


Fig. 11. Tracking results on soccer sequences, frame #246, 628, 630, 661, 686, 996, Green: IPCA, Red: our results. The IPCA started to drift off from frame #628 when the player's legs moved fast, and lost track shortly.

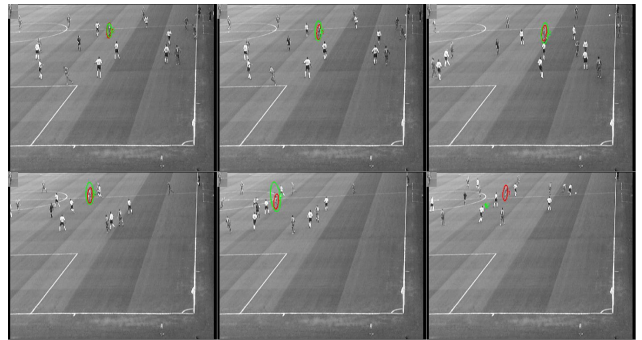


Fig. 12. Tracking results on soccer sequences, frame #10, 15, 122, 248, 285, 360, Green: IPCA, Red: our results. The IPCA started to drift off from frame #15 due to low contrast between the target and the background.

## ACKNOWLEDGMENTS

We would like to thank DSO National Laboratories, Singapore for partially sponsoring this work, and David Ross for sharing the test sequences.

## REFERENCES

- [1] V. Arsigny, P. Fillard, X. Pennec, N. Ayache, et al. Geometric means in a novel vector space structure on symmetric positive-definite matrices. *SIAM Journal on Matrix Analysis and Applications*, 29(1):328, 2008.



Fig. 13. Tracking results on DUDEK FACE sequences, frame #1, 361, 459, 605, 795, 1095, Green: IPCA, Red: our results. Both results were comparable despite of his rich facial expressions, which had more effects on our covariance descriptor.



Fig. 14. Tracking results on PETS2001 vehicle sequences, frame #1, 25, 50, 75, 100, 125, Green: IPCA, Red: our results. Both results were comparable.



Fig. 15. Tracking results on car sequences, frame #1, 132, 150, 168, 184, 227, Green: IPCA, Red: our results. The IPCA performed better, was robust to illumination changes, but our method mainly used template gradients, which changed dramatically due to shadow and lack of reflection of the car plate. At frame #227, the arrow sign might look too similar to the target in gradients.

- [2] M. Belkin and P. Niyogi. Laplacian eigenmaps for dimensionality reduction and data representation. *Neural computation*, 15(6):1373–1396, 2003.
- [3] S. Birchfield. Elliptical head tracking using intensity gradients and color histograms. In *CVPR*, pages 232–, 1998.
- [4] M. Black and A. Jepson. Eigentracking: Robust matching and tracking of articulated objects using a view-based representation. *IJCV*, 26(1):63–84, 1998.
- [5] O. Cappe, S. Godsill, and E. Moulines. An overview of existing methods and recent advances in sequential monte carlo. *Proceedings of the IEEE*, 95(5):899–924, May 2007.
- [6] P. C. Cargill, C. U. Rius, D. M. Quiroz, and A. Soto. Performance evaluation of the covariance descriptor for target detection. In *Chilean Computer Science Society (SCCC), 2009 International Conference of the*, pages 133–141, nov 2009.

- [7] C. Cedras and M. Shah. Motion-based recognition a survey. *Image and Vision Computing*, 13(2):129–155, 1995.
- [8] M. Chen, S. Pang, T. Cham, and A. Goh. Visual tracking with generative template model based on riemannian manifold of covariances. In *Information Fusion (FUSION), 2011 Proceedings of the 14th International Conference on*, pages 1–8. IEEE, 2011.
- [9] R. Collins, Y. Liu, and M. Leordeanu. Online selection of discriminative tracking features. *PAMI*, 27(10):1631–1643, 2005.
- [10] R. Cowie, E. Douglas-Cowie, N. Tsapatsoulis, G. Votsis, S. Kollias, W. Fellenz, and J. Taylor. Emotion recognition in human-computer interaction. *Signal Processing Magazine, IEEE*, 18(1):32–80, 2001.
- [11] N. Dalal and B. Triggs. Histograms of oriented gradients for human detection. In *CVPR*, volume 1, pages 886–893 vol. 1, June 2005.
- [12] P. T. Fletcher and S. Joshi. Riemannian geometry for the statistical analysis of diffusion tensor data. *Signal Processing*, 87(2):250–262, 2007.
- [13] W. Forstner and B. Moonen. A metric for covariance matrices. Technical report, Dept. of Geodesy and Geoinformatics, Stuttgart University, 1999.
- [14] A. Goh, C. Lenglet, P. Thompson, and R. Vidal. A non-parametric riemannian framework for processing high angular resolution diffusion images (hardi). In *CVPR*, pages 2496–2503, june 2009.
- [15] M. Grabner, H. Grabner, and H. Bischof. Learning features for tracking. In *CVPR*, pages 1–8. IEEE, 2007.
- [16] M. Isard and A. Blake. CONDENSATION - conditional density propagation for visual tracking. *IJCV*, 29:5–28, 1998.
- [17] K. Ito. The brownian motion and tensor fields on riemannian manifold. *Kiyosi Itô selected papers*, page 298, 1987.
- [18] O. Javed and M. Shah. Tracking and object classification for automated surveillance. *ECCV 2002*, pages 439–443, 2006.
- [19] A. Jepson, D. Fleet, and T. El-Maraghi. Robust online appearance models for visual tracking. *PAMI*, 25(10):1296–1311, oct 2003.
- [20] T. Kaneko and O. Hori. Template update criterion for template matching of image sequences. In *Pattern Recognition, 2002. Proceedings. 16th International Conference on*, volume 2, pages 1–5. IEEE, 2002.
- [21] J. Kruskal. Multidimensional scaling by optimizing goodness of fit to a nonmetric hypothesis. *Psychometrika*, 29(1):1–27, 1964.
- [22] V. Manohar, P. Soundararajan, H. Raju, D. Goldgof, R. Kasturi, and J. Garofolo. Performance evaluation of object detection and tracking in video. *Computer Vision-ACCV 2006*, pages 151–161, 2006.
- [23] I. Matthews, T. Ishikawa, and S. Baker. The template update problem. *PAMI*, 26:810–815, 2004.
- [24] D. McKeown Jr and J. Denlinger. Cooperative methods for road tracking in aerial imagery. In *Computer Vision and Pattern Recognition, 1988. Proceedings CVPR'88., Computer Society Conference on*, pages 662–672. IEEE, 1988.
- [25] H. Nguyen, M. Worring, and R. Van Den Boomgaard. Occlusion robust adaptive template tracking. In *ICCV*, volume 1, pages 678–683. IEEE, 2001.
- [26] Y. Pang, Y. Yuan, and X. Li. Gabor-based region covariance matrices for face recognition. *Circuits and Systems for Video Technology, IEEE Transactions on*, 18(7):989–993, 2008.
- [27] X. Pennec. Intrinsic statistics on riemannian manifolds: Basic tools for geometric measurements. *J. Math. Imaging Vis.*, 25:127–154, July 2006.
- [28] X. Pennec, P. Fillard, and N. Ayache. A riemannian framework for tensor computing. *IJCV*, 66:41–66, 2006.
- [29] F. Porikli. Integral histogram: a fast way to extract histograms in cartesian spaces. In *CVPR*, volume 1, pages 829–836 vol. 1, 2005.
- [30] F. Porikli and T. Kocak. Robust license plate detection using covariance descriptor in a neural network framework. In *Video and Signal Based Surveillance, 2006. AVSS'06. IEEE International Conference on*, pages 107–107. IEEE, 2006.
- [31] F. Porikli, O. Tuzel, and P. Meer. Covariance tracking using model update based on lie algebra. In *CVPR*, volume 1, pages 728–735, june 2006.
- [32] Y. Rathi, A. Tannenbaum, and O. Michailovich. Segmenting images on the tensor manifold. In *CVPR*, pages 1–8, june 2007.
- [33] B. Ristic, S. Arulampalam, and N. Gordon. *Beyond the Kalman Filter: Particle Filters for Tracking Applications*. Artech House, 2004.
- [34] D. Ross, J. Lim, R.-S. Lin, and M.-H. Yang. Incremental

- Learning for Robust Visual Tracking. *IJCV*, 77(1):125–141, 2008.
- [35] S. Roweis and L. Saul. Nonlinear dimensionality reduction by locally linear embedding. *Science*, 290(5500):2323–2326, 2000.
- [36] A. Schwartzman. *Random ellipsoids and false discovery rates: Statistics for diffusion tensor imaging data*. PhD thesis, Stanford University, 2006.
- [37] M. B. Stegmann. Object tracking using active appearance models. *Proc. 10th Danish Conference on Pattern Recognition and Image Analysis*, pages 54–60, 2001.
- [38] F. Suard, A. Rakotomamonjy, A. Bensrhair, and A. Broggi. Pedestrian detection using infrared images and histograms of oriented gradients. In *Intelligent Vehicles Symposium, 2006 IEEE*, pages 206–212. Ieee, 2006.
- [39] J. Tenenbaum, V. De Silva, and J. Langford. A global geometric framework for nonlinear dimensionality reduction. *Science*, 290(5500):2319–2323, 2000.
- [40] O. Tuzel, F. Porikli, and P. Meer. Region covariance: A fast descriptor for detection and classification. *ECCV*, pages 589–600, 2006.
- [41] O. Tuzel, F. Porikli, and P. Meer. Region Covariance: A Fast Descriptor for Detection and Classification. In A. Leonardis, H. Bischof, and A. Pinz, editors, *ECCV 2006*, volume 3952 of *Lecture Notes in Computer Science*, pages 589–600. Springer Berlin / Heidelberg, 2006.
- [42] O. Tuzel, F. Porikli, and P. Meer. Human detection via classification on riemannian manifolds. In *CVPR*, pages 1 – 8, june 2007.
- [43] O. Tuzel, F. Porikli, and P. Meer. Pedestrian detection via classification on riemannian manifolds. *PAMI*, 30(10):1713 – 1727, oct. 2008.
- [44] G. Wang, Y. Liu, and H. Shi. Covariance tracking via geometric particle filtering. In *Intelligent Computation Technology and Automation, 2009. ICICTA '09. Second International Conference on*, volume 1, pages 250 –254, 2009.
- [45] Y. Wu, H. Ling, E. Blasch, L. Bai, and G. Chen. Visual tracking based on log-euclidean riemannian sparse representation. *Advances in Visual Computing*, pages 738–747, 2011.
- [46] A. Yilmaz, O. Javed, and M. Shah. Object tracking: A survey. *ACM Comput. Surv.*, 38(4), 2006.
- [47] X. Zhan. Extremal eigenvalues of real symmetric matrices with entries in an interval. *SIAM journal on matrix analysis and applications*, 27(3):851–860, 2006.

**Dr. Pang Sze Kim** is a principal member of technical staff and currently is the head of Signal Processing Laboratories at DSO National Laboratories. Sze Kim obtained his Ph.D. from University of Cambridge.

777  
778

**DR. Alvina Goh** obtained her Ph.D. from the Department of Biomedical Engineering at the Johns Hopkins University in May 2010. Currently, she is a researcher at the DSO National Labs and an adjunct assistant professor in the Department of Mathematics at the National University of Singapore. Her research interests include machine learning, computer vision, and medical imaging.

779  
780  
781  
782  
783  
784

**Marcus Chen** is a PhD student in the School of Computer Engineering, Nanyang Technological University, and member of technical staff in DSO National Laboratories. He received his B.S. in Electrical and Computer Engineering with university honours in 2007 from Carnegie Mellon University, and M.S. in Electrical Engineering from Stanford University in 2008.

**Dr. Cham Tat Jen** is an Associate Professor in the School of Computer Engineering, Nanyang Technological University, and Director of the Centre for Multimedia & Network Technology (CeMNet). He received his BA in Engineering with triple first class honours in 1993 and his PhD in 1996, both from the University of Cambridge, during which he was awarded the Loke Cheng-Kim Foundation Scholarship, the Alexandria Prize, the Engineering Members Prize as well as the St Catharines College Senior and Research Scholarships. Tat-Jen was subsequently conferred a Jesus College Research Fellowship in Science in 1996-97. From 1998 to 2001, he was a research scientist at DEC/Compaq CRL in Cambridge, MA, USA, where his experience included technology transfer to product groups and showcasing research work to Hollywood studios. After joining NTU in 2002, he was concurrently a Faculty Fellow in the Singapore-MIT Alliance Computer Science Program in 2003-2006.

760  
761  
762  
763  
764  
765  
766  
767  
768  
769  
770  
771  
772  
773  
774